ACS SENSORS

pubs.acs.org/acssensors

Article

Improving Sensitivity and Reproducibility of Surface-Enhanced Raman Scattering Biochips Utilizing Magnetoplasmonic Nanoparticles and Statistical Methods

Chin-Wei Lin, Li-Yu Chen, Yu-Ching Huang, Pradeep Kumar, Yu-Zhi Guo, Chiu-Hsien Wu, Li-Min Wang, and Kuen-Lin Chen*

Cite This: *ACS Sens.* 2024, 9, 305−314

Read Online

ACCESS | Metrics & More | Article Recommendations | Supporting Information

ABSTRACT: Surface-enhanced Raman scattering (SERS) technology has been widely recognized for its remarkable sensitivity in biochip development. This study presents a novel sandwich immunoassay that synergizes SERS with magnetoplasmonic nanoparticles (MPNs) to improve sensitivity. By taking advantage of the unique magnetism of these nanoparticles, we further enhance the detection sensitivity of SERS biochips through the applied magnetic field. Despite the high sensitivity, practical applications of SERS biochips are often limited by the issues of stability and reproducibility. In this study, we introduced a straightforward statistical method known as "Gaussian binning", which involves initially binning the two-dimensional Raman mapping data and subsequently applying Gaussian fitting. This approach enables a more consistent and reliable interpretation of data by reducing the variability inherent in Raman signal measurements. Based on our method, the biochip, targeting for C-reactive protein (CRP), achieves an impressive detection limit of 5.96 fg/mL, and with the application of a 3700 G magnetic field, it further enhances the detection limit by 5.7 times, reaching 1.05 fg/mL. Furthermore, this highly sensitive and magnetically tunable SERS biochip is easily designed for versatile adaptability, enabling the detection of other proteins. We believe that this innovation holds promise in enhancing the clinical applicability of SERS biochips.

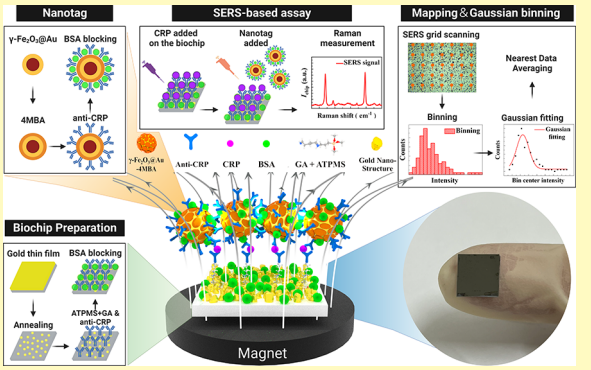

KEYWORDS: *biosensors, sensitive detection, reproducibility, surface-enhanced Raman scattering (SERS), magnetoplasmonic nanoparticles (MPNs), C-reactive protein (CRP)*

Downloaded via CHANG GUNG UNIV on May 16, 2024 at 08:40:02 (UTC).
See https://pubs.acs.org/sharingguidelines for options on how to legitimately share published articles.

Surface-enhanced Raman scattering (SERS), which leverages surface plasmon resonance, amplifies the Raman signal by intensifying the electric field around the analyte. The intensity of these signals can be magnified by several orders of magnitude, from billions up to trillions of times.[1,2] SERS enhancement manifests in two forms: Electromagnetic enhancement, driven by localized surface plasmon resonance (LSPR), is a result of light irradiation on a metal surface with nanostructures. This process creates an effective electromagnetic field that can significantly amplify the Raman scattering signal of the analyte with an amplification factor of approximately 10^{11} times.[2−6] Chemical enhancement, while less effective, originates from direct interaction between the analyte or Raman tags and the metal surface. This interaction reinforces the Raman signal through charge transfer and coupling, leading to an increase ranging around 10 to 10^3 times.[6−9]

To enhance the SERS performance, researchers are increasingly focusing on nanomaterials. Favored for their stability and easy synthesis, gold nanoparticles (Au NPs) effectively enhance SERS effectiveness and enable specific biomolecule detection.[10−14] Magnetoplasmonic nanoparticles (MPNs), which combine a magnetic core with a noble metal shell, extend these benefits and offer additional advantages in biomedical applications like magnetic drug delivery,[15] magnetic resonance imaging,[16] and even in SERS. MPNs can facilitate separation and enrichment of the analyte through a magnetic field, thereby improving the sensitivity. Besides, under an external magnetic field, these MPNs can aggregate and increase the density of the SERS hot spots, further enhancing the detection limit (LOD).[17−19] Recent research indicates that magnetic SERS could possess high sensitivity and great potential in biosensing. For instance, Liu's team employed a lateral flow immunoassay with multichannel SERS

Received: September 23, 2023
Revised: December 3, 2023
Accepted: December 28, 2023
Published: January 15, 2024

ACS Publications

© 2024 American Chemical Society

and magnetic SERS tags for H1N1, SARS-CoV-2, and RSV detection, achieving LODs of 85 copies/mL for H1N1 and 8 pg/mL for SARS-CoV-2 and RSV.[20] Yin et al. employed a magnetic-responsive SERS biosensor utilizing Au NPs/rGO and SPION/Au NPs substrates for the detection of SARS-CoV-2's N-cDNA, achieving a remarkable 10-fold improvement in the detection limit, from 1 fM to 100 aM.[21] Despite advancements, SERS technology faces challenges like uneven analyte distribution and poor reproducibility.[2,7,19,22,23] The objective of this work is to develop a novel methodological framework and biochip architecture that utilizes the unique properties of MPNs to enhance SERS-based detection, enabling highly sensitive analysis of analytes.

Our study employs a sandwich immunoassay method that combines MPNs with a SERS biochip. This approach involves coupling Raman tags to MPNs, which are then bound to the target proteins on the biochip. The biochip's enhancement is reliant on hot spot behavior, intricately linked to LSPR. Upon exposure to incident light that matches the resonant frequency of a plasma, metallic nanoparticles undergo a collective electron oscillation. This oscillation subsequently results in the radiation of a dipole field that interacts with the original electric field induced by the incident light. This interaction leads to a transformation and redistribution of the local electric field around the nanoparticles. Consequently, there is a significant amplification of the electric field at specific positions near the nanoparticles, termed hot spots. Molecules that are located or adsorbed near these hot spots are subjected to an intensified electric field, thereby leading to a substantial enhancement of their Raman signal.[19,24]

The MPNs used in our study exhibit both magnetic and plasmonic properties. The external magnetic field can induce the magnetic response of the MPNs, causing them to aggregate and decreasing the distance between the particles. This reduction in the interparticle distance significantly amplified the electric field between them.[25] This intensified electric field can further enhance the Raman signal. The diagram of the magnetic SERS biochip is visualized in Figure 1.

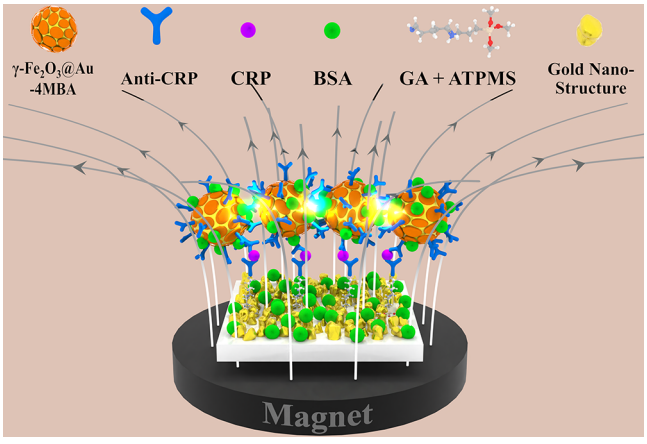

Figure 1. Schematic diagram of the magnetically enhanced SERS biochip. Different particle representations are provided at the top of the figure. In GA and APTMS, the atoms colored red, blue, gray, light orange, and white correspond to oxygen, nitrogen, carbon, silicon, and hydrogen molecules, respectively. The glowing areas between NPs indicate hot spots, and the gray lines with arrows depict the magnetic field lines.

Significant signal variations have also been observed in our SERS measurements. In our approach to overcome reproducibility challenge in SERS, we perform statistical analysis of the Raman intensity at different locations on the biochip. Contrary to artificially engineering orderly arranged surfaces,[26−29] our approach allows the natural distribution of biomolecules. This approach leads to a distribution that typically follows a Gaussian pattern. We thus propose that the Gaussian distribution aptly describes the intensity distribution across the biochip, and consequently, the intensities around the Gaussian central peak should be indicative of the biochip's representative intensity. This approach can better interpret the data and obtain consistent results across different biochips.

Expanding on this foundation, this study specifically focuses on C-reactive protein (CRP), a biomarker of substantial clinical importance. CRP, produced by the liver, elevates in response to inflammation, infection, or injury, serving as a vital indicator for assessing the body's inflammatory response.[30] In addition to cardiovascular disease, researchers have recently explored the application of CRP in assessing other diseases, including neurodegenerative diseases and cancer.[31,32] Our previous work developed a sensitive immunoassay platform using the magneto-optical Faraday effect and biofunctionalized magnetic nanoparticles, achieving an LOD of 0.53 ng/mL for the CRP assay.[33] Extending from our previous work, we have developed a magnetic SERS technique via MPNs, achieving an enhanced LOD of 1.05 fg/mL under an applied magnetic field.

EXPERIMENTAL SECTION

This study utilized a sandwich immunoassay approach. The γ-Fe_2O_3@Au core/shell MPNs, functionalized with 4-mercaptobenzoic acid (4MBA) were used as the primary reagent, also referred to as SERS nanotags in the following. In SERS measurements, 4MBA serves as the target molecule. The SERS immunochip comprises a 1 cm × 1 cm (100) silicon chip with island-like gold nanostructures on its surface. Gold nanostructures were fabricated by using DC sputtering, followed by an annealing process. The annealed gold films would form nanoislands, which were distributed across the substrate surface.[34,35] These gold nanostructures are designed to facilitate uniform surface modification, avoiding the aggregation and uneven clustering of functional molecules. Additionally, they have the potential to form hot spots with the MPNs above, thereby increasing the hot spot density. 3-Aminopropyltriethoxysilane (APTMS) is employed to introduce primary amine functionalities onto the silica surface. Following this, glutaraldehyde (GA) serves as a cross-linking agent, facilitating covalent attachment between these surface-bound amines and specific proteins. Bovine serum albumin (BSA) is used as a blocking agent to reduce nonspecific adsorption by occupying potential nonspecific binding sites on the biochip. Further details on the preparation of the MPNs, SERS nanotags, and SERS immunochip, along with information on materials and chemicals, are available in the Supporting Information.

SERS-Based Sandwich Immunoassay Process. Figure 2 presents a flowchart that illustrates both the reagent and biochip preparation processes, as well as the operational principles of the SERS-based immunoassay method. The assay process commences by adding 50 μL of the sample to the prepared biochip, followed by incubation at 37 °C for 30 min. After incubation, the biochip undergoes a washing step with pH 7.4 phosphate buffered saline (PBS) and DI water. Next, 40 μL of the prepared nanotags is applied to the chip, which is then incubated at 4 °C for 2 h. In the final step, the biochip is washed again with pH 7.4 PBS buffer and DI water to prepare it for the SERS measurement. Details about the incubation and washing procedures are comprehensively listed in the Supporting Information. If CRP is present in the testing sample, then the CRP antibodies affixed to the chip will bind and immobilize the CRP on

https://doi.org/10.1021/acssensors.3c02007
ACS Sens. 2024, 9, 305−314

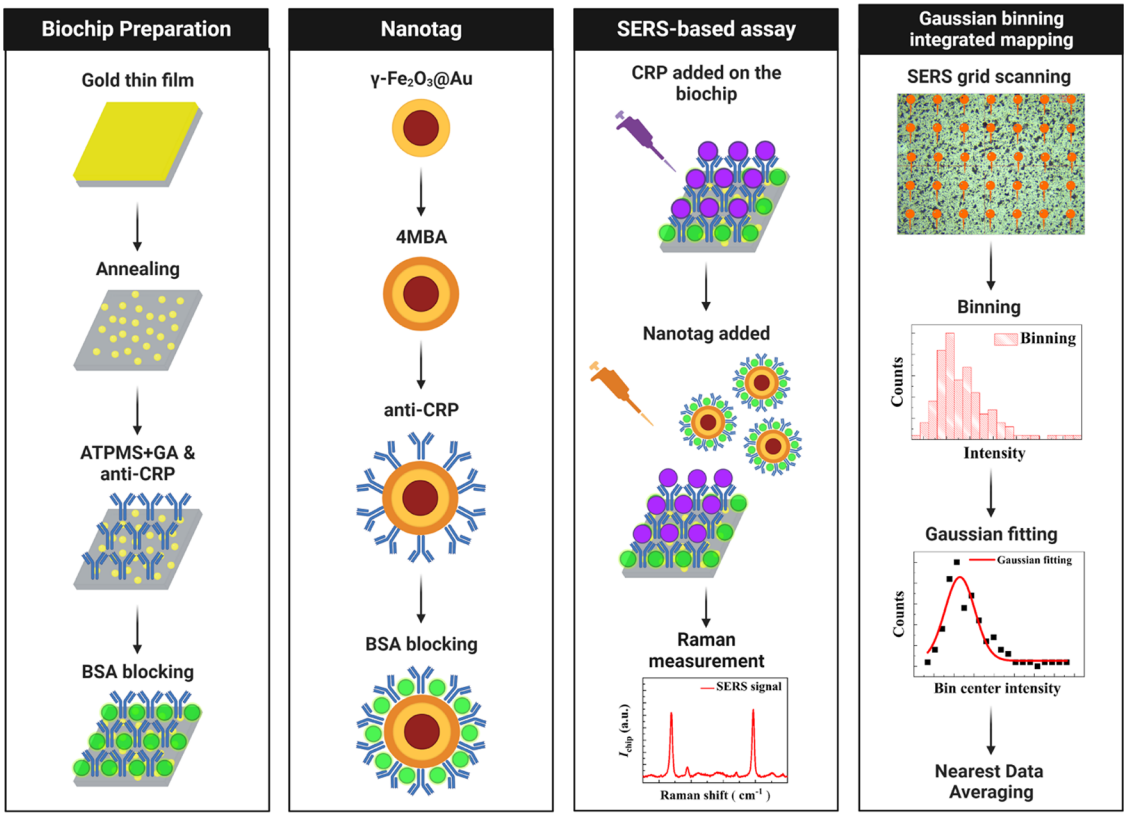

Figure 2. Schematic illustration of our SERS-based immunoassay (created with BioRender.com).

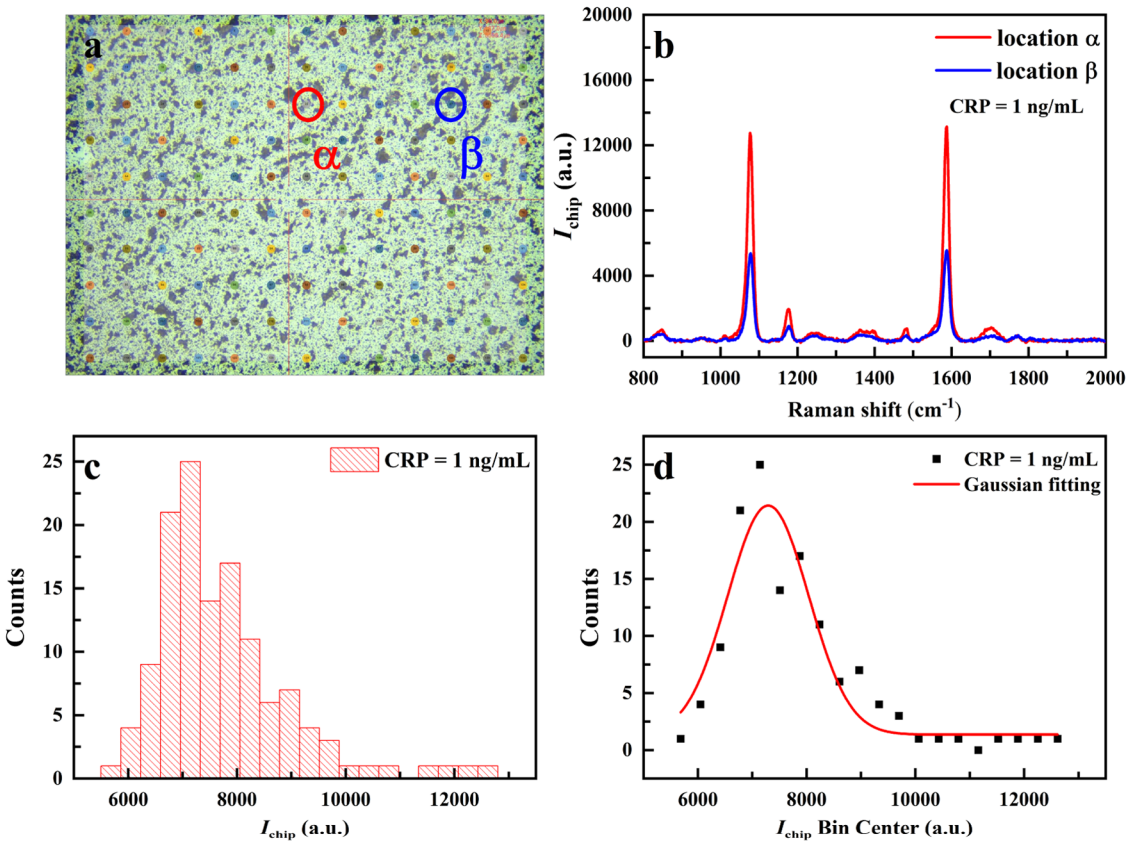

Figure 3. (a) Optical imaging of the biochip in SERS measurement and 130 measurement points on the chip (Random color points). (b) SERS signals measured from locations α and β. The CRP concentration used in this test is 1 ng/mL. (c) Data of 130 points were classified into 20 predetermined groups for further statistics. (d) Gaussian function fitting of the distribution of 20 groups data.

https://doi.org/10.1021/acssensors.3c02007
ACS Sens. 2024, 9, 305−314

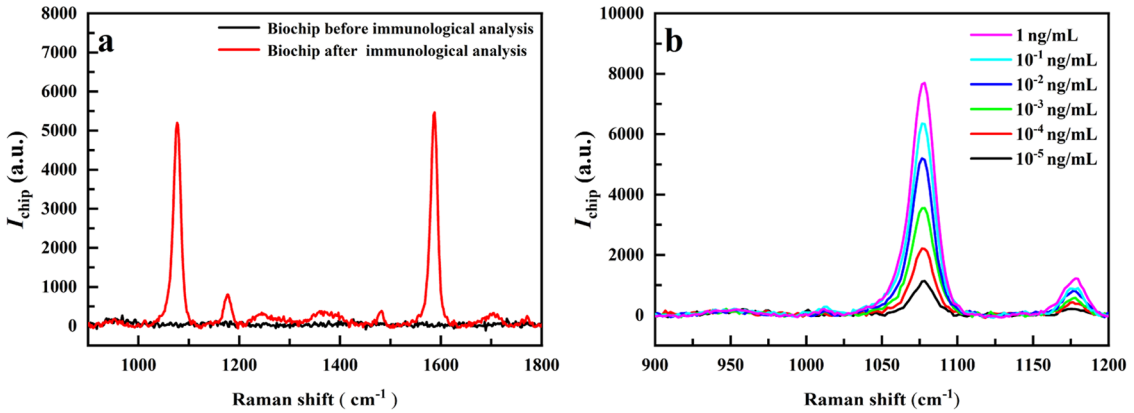

Figure 4. (a) SERS signal before and after immunological analysis. (b) SERS signals of the biochip at different CRP concentrations.

the chip surface. Following this, the addition of the reagent, consisting of γ-Fe_2O_3@Au nanoparticles functionalized with anti-CRP, enables a reaction with CRP, leading to their subsequent immobilization on the chip surface. Clearly, an increase in the concentration of CRP leads to a corresponding increase in the number of γ-Fe_2O_3@Au nanoparticles adhering to the chip surface. Additionally, 4MBA serves as a Raman tag to quantify γ-Fe_2O_3@Au nanoparticles by measuring the Raman signal intensity. This method facilitates the quantitative determination of the CRP concentration based on the Raman signal of 4MBA on the γ-Fe_2O_3@Au nanoparticles.

Raman Signal Measurement. SERS signal measurements were conducted using a 633 nm excitation laser and recorded with a Raman spectrometer (NS220 single laser micro-Raman spectrometer, Nanoscope Systems, Inc., Daejeon, Korea). A laser output power of 0.2 mW was used, along with an acquisition time of 1 s and 2 accumulations. Higher laser energies were avoided to prevent potential damage to the proteins. Baseline correction was applied for the final spectra via the background subtracted. Additionally, a 2D mapping function defined an area of 480 μm × 360 μm, with 40 μm point spacing, to collect data from 130 points for subsequent analysis. The measurement points are visually represented by random color points in Figure 3a.

A significant challenge in SERS measurements is reproducibility,[7,19,23,36] as evidenced by the variation in signal intensity at different measurement points. Figure 3b shows the SERS signals from locations α and β, indicated by the red and blue circles, respectively, in Figure 3a. Besides, the Raman intensity distribution of the 2D mapping exhibits a relative standard deviation (RSD) of 22.6% (Figure S1). It can be clearly observed that the uneven distribution of particles on the chip's surface results in varying intensities of measured SERS signals in different regions. Therefore, in this experiment, a Gaussian binning method is proposed to address this issue by gathering and statistically analyzing data from various locations.

Data from 130 points, focusing on the 1076.5 cm^{-1} peak of 4MBA, were grouped for statistical analysis. Then, the data of the 1076.5 cm^{-1} peak from 130 locations were organized into 20 predetermined groups by signal intensity as shown in Figure 3c. After statistical analysis, the data showed a normal distribution with the intensity values tending to cluster around a specific average. This could conform to the central limit theorem, suggesting that regardless of the population's distribution, the sampling distribution of the mean tends to approximate a normal distribution with a large sample size. Hence, the application of a Gaussian distribution is a suitable approach for statistical analysis.

Gaussian curve fitting was applied to the binned data, as shown in Figure 3d, to determine the central SERS intensity of the 1076.5 cm^{-1} peak, denoted as I_{Gpeak}. Next, we selected the data of 15 points, of which the SERS intensity is closest to I_{Gpeak} and calculated the average intensity of these 15 points, which served as the characteristic SERS intensity for this chip, denoted as I_{chip}. It is worth mentioning that the smaller the sigma value in the fitted Gaussian curve, the sharper the peak of the Gaussian curve, indicating that the signal distribution on this chip is more uniform. Therefore, the fitted Gaussian curve can serve as a quality indicator for the biochip. The flowchart of our Gaussian binning integrated with the two-dimensional mapping method is also illustrated in Figure 2.

RESULTS AND DISCUSSION

Characterization of the SERS Nanotags and SERS Immunochips. The nanotags' preparation at each step was verified using UV−vis spectrophotometry (Figure S2). In the TEM images, the γ-Fe_2O_3@Au nanoparticles, used for fabricating the SERS nanotags, exhibit a diameter of approximately 25 nm. The external layer, believed to be gold, had a crystal lattice constant of 0.235 nm, while the inner layer, believed to be γ-Fe_2O_3, had a lattice constant of 0.295 nm (Figure S3). The average hydrodynamic diameter of γ-Fe_2O_3@Au in water is 61.0 nm, with a polydispersity index (PI) of 0.214 and zeta potential of −49.9 mV (Figure S4). Regarding the SERS immunochip verification, SEM imaging revealed gold nanostructures on the silicon substrate, approximately 10 nm in size. After the immunoassay, the element distribution of the SERS immunochip was analyzed using energy-dispersive X-ray spectroscopy (EDS) mapping (Figure S5). EDS results, when observed at a larger scale, indicated a uniform distribution of materials across the chip's surface, consistent with the anticipated results of the fabrication process. Nonetheless, a detailed analysis at a finer scale reveals the presence of localized areas still exhibiting nonuniformity. These irregularities in material distribution contribute to variations in signal intensity, which in turn impacts the reproducibility of SERS chips. Details regarding the characterization of the SERS nanotags and SERS immunochip can be found in the Supporting Information.

Measurement and Analysis of Biochips. The 4MBA molecules linked on the gold surfaces contribute to two distinct SERS peaks at 1076.5 and 1587.5 cm^{-1}. The 1076.5 cm^{-1} peak originates from the benzene ring's breathing mode coupled with ν(C−S), and the 1587.5 cm^{-1} peak arises from the ν(C−C) vibration mode of the benzene ring.[37,38] 4MBA was exclusively present on the nanotags during the experiment. In essence, the successful binding of nanotags on the chip via the target is necessary to observe the two distinct SERS peaks of 4MBA at 1076.5 and 1587.5 cm^{-1}. Figure 4a displays the SERS spectra of the biochip before and after the immunoassay process. It is evident that the untreated biochip does not exhibit the SERS signal of 4MBA. However, the chip used in the immunoassay demonstrates two distinct SERS peaks of

https://doi.org/10.1021/acssensors.3c02007
ACS Sens. 2024, 9, 305−314

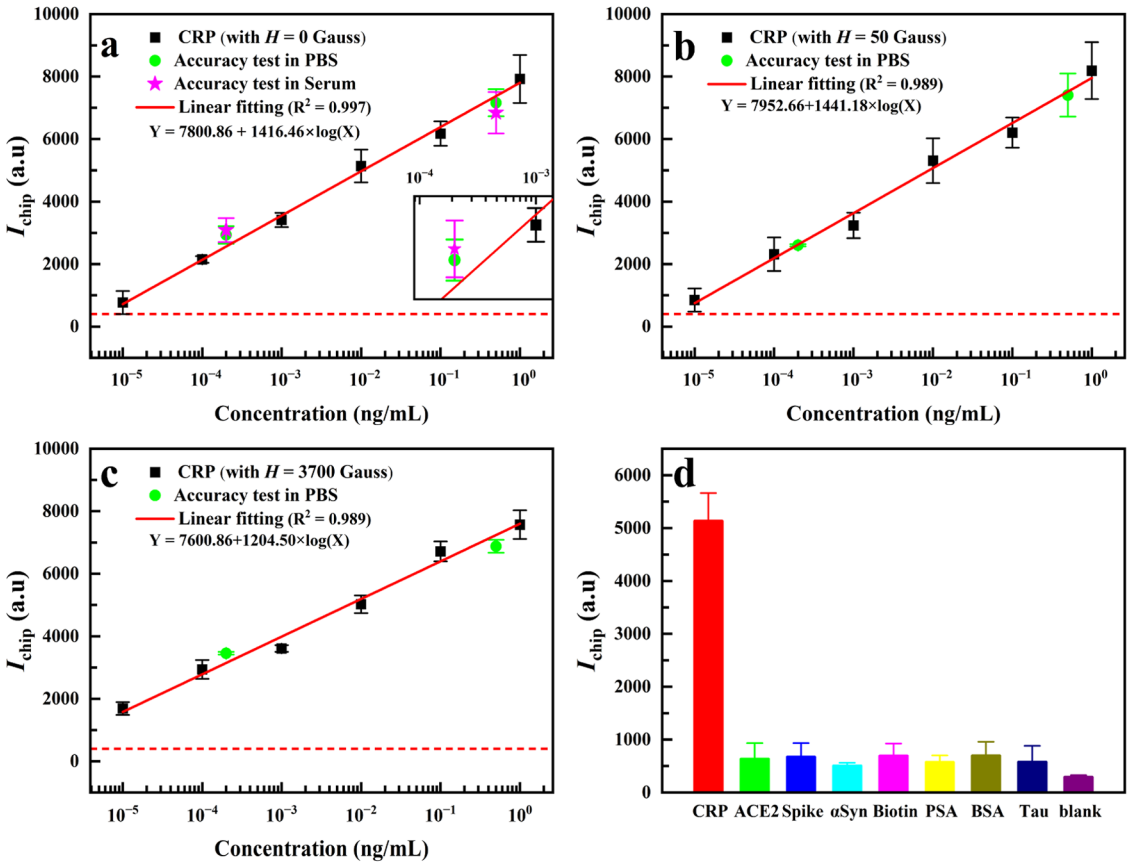

Figure 5. Relationship between the calculated SERS intensity I_{chip} and the logarithm of CRP concentrations under the applied magnetic fields of (a) normal conditions, (b) 50 G and (c) 3700 G. The red line is the linear fitting curve of the data, and the dashed line represents the minimum detectable signal X_m. The green points are two testing CRP concentrations (0.5 ng/mL and 2×10^{-4} ng/mL) in PBS and the magenta points indicate tests in human serum. The data were obtained from triplicate experiments and are shown as mean ± standard deviation. (d) Specificity test of our biochips.

4MBA at 1076.5 and 1587.5 cm^{-1}. This observation indicates the successful binding of nanotags on the chip via CRP during the immunoassay process. As explained in the chip design section, the number of nanotags on the chip is directly correlated to the biotarget concentration. The peak at 1076.5 cm^{-1} corresponds to the breathing mode coupled with the C−S bond, which is a moiety in thiolate compounds adhering to gold surfaces. Therefore, the 1076.5 cm^{-1} SERS peak of 4MBA was utilized in later experiments to quantify the CRP concentration.

Figure 4b illustrates the variation in the strength of the SERS peak at 1076.5 cm^{-1} as a function of the different CRP concentrations. The observed variation in the SERS signal with CRP concentration confirms the realization of the biochip's design concept. With an increased concentration of CRP in the sample, a larger number of nanotags bind to the chip surface, resulting in a stronger SERS signal from the 4MBA molecules. For different CRP concentrations, three different biochips were used to conduct three replicate experiments, and each biochip was subjected to 2D scanning measurements of 130 points. After data analysis of triplicate experiments, Figure 5a shows the correlation between the SERS intensity I_{chip} and the CRP concentration. It is shown that the SERS intensity I_{chip} linearly changes with the logarithm of the CRP concentration over a considerable concentration range ($1-10^{-5}$ ng/mL). To estimate the LOD, the guidelines defined by the International Union of Pure and Applied Chemistry (IUPAC) were followed.[39] X_m represents the minimum detectable signal strength of the system and is determined by the following equation

$$X_m = X_b + 3S_b \quad (1)$$

Here, X_b represents the blank signal and S_b denotes the standard deviation of the blank signal. Utilizing the linear fitting curve in Figure 5a and the value of X_m, the estimated LOD for our method is 5.96 fg/mL. In addition, it is noteworthy that the biochips we used in the triplicate experiments were prepared on three different days.

Raman Measurement with the External Magnetic Field. Building on our reagent design, which includes MPNs with both LSPR and magnetic properties, we investigated the impact of a magnetic field on our biochip's performance. For SERS measurements, a magnetic coil or a magnet was positioned beneath the biochip, applying a magnetic field perpendicular to its surface. A neodymium magnet generating a 3700 G field and a magnetic coil producing a 50 G field were utilized, both corresponding in size to the biochip. The magnetic field was maintained during the SERS measurement. The measurement area, located at the center of the biochip, occupies approximately 0.2% of the total chip size. Consequently, the magnetic field distribution across each measurement location on the biochip can be regarded as nearly uniform. To elucidate the effects of the magnetic field, we also prepared chips coated with biomaterial (CRP & anti-CRP) but

https://doi.org/10.1021/acssensors.3c02007
ACS Sens. 2024, 9, 305−314

without nanotags to examine the SERS signals under the influence of the magnetic field. The experimental results clearly demonstrated that, in the absence of nanotags, the SERS signals from the silicon substrate and biomaterials are almost unaffected by the magnetic field. Hence, it is evident that the previously observed SERS signals affected by the magnetic field originate from the magnetic nanotags (Figure S6). Figure 5b,c shows the relationship between the calculated SERS intensity I_{chip} and the logarithm of CRP concentrations under the applied magnetic fields of 50 and 3700 G, respectively. The data distribution patterns remain substantially consistent under the influence of the magnetic field. However, the SERS signal strength is enhanced by the magnetic field, with more pronounced effects observed under the stronger 3700 G field. The calculated LOD for the magnetic field of 50 G is approximately 5.74 fg/mL. On the other hand, the calculated LOD for the magnetic field of 3700 G is significantly improved to 1.05 fg/mL due to the stronger SERS enhancement.

To demonstrate the efficacy of the Gaussian binning method that we employed in improving the reproducibility issues in SERS chip measurements, we also utilized data from single-point measurements in the triplicate experiments for analysis (Figure S7). The analysis results revealed that the distribution of data from single-point measurements is less linear and more dispersed, with a larger standard error. The data from single-point measurements faithfully represented the persistent challenge of poor reproducibility among different SERS chips, highlighting noticeable differences in SERS signals even under identical experimental conditions. However, the application of the Gaussian binning method produced more consistent results across various biochips and exhibited good performance in the recovery percentage of CRP assays. This method could provide a better interpretation of the data and improve the reproducibility across different biochips.

Percentage of Recovery and Specificity Tests. To evaluate the clinical applicability of our method, tests were conducted, focusing on the percentage of recovery and specificity. Two CRP samples, one with a concentration of 0.5 ng/mL and the other with 2×10^{-4} ng/mL, were analyzed using our biochip under magnetic fields. We also conducted tests for CRP detection in processed human serum. The test results in PBS, depicted as the green dots in Figure 5a−c, correspond to the experiments conducted under normal conditions, 50 G, and 3700 G magnetic fields, respectively. The inset in Figure 5a presents a magnified view. It is evident that the test results closely align with the calibration curve under every experimental condition. The percentage of recovery is defined as the ratio of I_{test} to I_{cal}, where I_{test} represents the measured SERS intensity of the test sample and I_{cal} denotes the calculated SERS intensity of the test sample obtained from the calibration curve. The results of the percentage of recovery are shown in Table 1. In the higher CRP concentration sample (0.5 ng/mL), the lowest observed percentage of recovery on our biochip still exceeded 95.0%. However, for the sample with an ultralow CRP concentration (2×10^{-4} ng/mL), the worst assay percentage of recovery slightly declines to 85.5%. This decrease in the percentage of recovery could be attributed to the lower signal-to-noise ratio (SNR) of the SERS signal due to the weaker SERS intensity of our biochip triggered by the ultralow CRP concentration. Notably, the highest percentage of recovery for both concentrations was observed at a 50 G magnetic field. The magnetic field induces particle agglomeration, thereby enhancing hot spots and improving sensitivity. However, this agglomeration could also lead to uneven hot spot distribution, consequently affecting the percentage of recovery of the test. It is reasonable to infer that there might be an optimal range of magnetic field strength where the percentage of recovery of the measurement is maximized. Nonetheless, it is noteworthy that the results of the recovery test at a higher magnetic field still maintain above 90%.

Table 1. Percentage of Recovery of the CRP Assay Using Our Biochip under Normal Conditions and with Applied Magnetic Fields

CRP concentration	0.5 ng/mL (in PBS)	2×10^{-4} ng/mL (in PBS)
H = 0 G	97.1 ± 5.9%	85.5 ± 10.9%
H = 50 G	98.5 ± 9.2%	99.2 ± 1.4%
H = 3700 G	95.0 ± 2.9%	90.1 ± 1.4%

The results of CRP in the processed human serum are denoted by magenta stars in Figure 5a. For the higher concentration of 0.5 ng/mL, there is a deviation of 4.5% from the PBS results, while the lower concentration of 2×10^{-4} ng/mL shows a deviation of 5.2%. These discrepancies may arise from the matrix effects of serum, potentially influencing outcomes differently than PBS. While this deviation indicates room for optimization, considering the inherent complexities and potential interferences associated with serum relative to PBS, the results remain promising. The performance in percentage of recovery of the CRP assay showcases the robustness of the biochip.

To evaluate the specificity of our biochip, we conducted tests using CRP and several other common proteins, including angiotensin-converting enzyme 2 (ACE2), spike protein of SARS-CoV-2, α-synuclein, biotin, prostate-specific antigen (PSA), bovine serum albumin (BSA), and tau protein. Each protein was prepared at a concentration of 10^{-2} ng/mL for sample preparation, and the measurement results are depicted in Figure 5d. The results revealed that only CRP triggered a notable chip reaction, leading to a stronger SERS signal, while the SERS signals for the other proteins remained comparable to the blank signal. These findings demonstrate the excellent specificity of our chip design, effectively mitigating the influence of nontargeted proteins. Furthermore, the results obtained from the percentage of recovery and specificity tests strongly indicate the promising potential of our SERS biochip for clinical applications.

Analysis of the Enhancement of Magnetic SERS Biochips. To elucidate the enhancement mechanism, we applied the following formula[40] to assess the enhancement factor (EF) of our biochip under magnetic fields

$$\mathrm{EF} = \frac{(I_m/C_m)}{(I_0/C_0)} \tag{2}$$

In this formula, I_m is the SERS intensity with the biochip under a magnetic field, while C_m denotes the corresponding target concentration, which is CRP in our analysis, attributed to its positive correlation with 4MBA. I_0 and C_0 denote the SERS intensity and target concentration of the biochip without a magnetic field, respectively. For the EF calculation relative to the CRP concentration, we supposed that C_m and C_0 are equal because the CRP concentration should not be influenced by the applied magnetic field.

https://doi.org/10.1021/acssensors.3c02007
ACS Sens. 2024, 9, 305−314

As shown in Figure 6, SERS enhancement of the biochip due to magnetic fields varies with the CRP concentrations. At

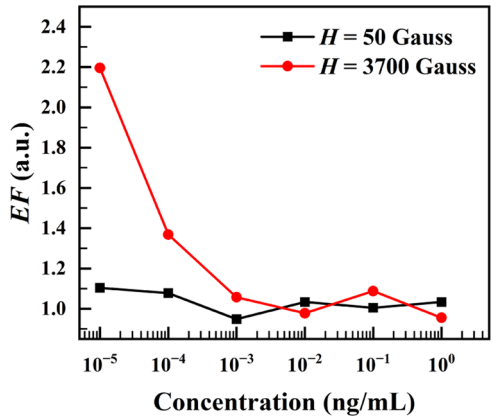

Figure 6. EF value of the biochip at different CRP concentrations under magnetic fields of 50 and 3700 G.

higher CRP concentrations, the EF tends toward 1, reflecting small enhancements. At lower concentrations, there is a notable increase in the EF value, particularly under stronger magnetic fields. This behavior occurs because of the high density of MPNS at higher CRP concentrations; the distance between each bound MPN is already minimal. Therefore, even in the presence of an external magnetic field, they cannot converge any closer to amplify the hot spot. In contrast, at lower concentrations, where there are fewer bonded MPNS and larger interparticle spacing, magnetic fields can effectively gather MPNS, shortening their spacing and consequently amplifying the SERS signal. The trends observed in the slopes of CRP calibration curves when subjected to different magnetic fields are also similar to the behavior of EF. At lower CRP concentrations, there is a noticeable increase in SERS signal intensity, but this increment is not noticeable at higher CRP concentrations. This effect produces a flatter calibration curve and consequently results in a lower LOD. By capitalizing on the unique properties of MPNs and manipulating their interparticle distance through an external magnetic field, our approach enhances the SERS signal of low CRP concentrations and improves the LOD of our biochip.

Besides, we also measured the blocking temperature with respect to magnetic field $T_B(H)$ to estimate the aggregation of MPNs on the biochip induced by the magnetic field.[41,42] The experimental data of $T_B(H)$ showed that the aggregation behavior of the MPNs on the biochip satisfies the interparticle interaction model (Figure S8). Based on the interparticle interaction model, we can obtain a correlation length within which the magnetization fluctuations are correlated. For the biochip accomplished the assay of 2×10^{-4} ng/mL CRP, the derived correlation length L_H of MPNs is approximately 35 nm at a field of 50 G and 26 nm at 3700 G. The decrease in L_H proved that the applied magnetic field indeed induces aggregation of MPNs on the biochips.

Comparison of Others Works. Currently, the detection limit of CRP in conventional enzyme-linked immunosorbent assay (ELISA) can reach the level of 0.1 ng/mL.[43,44] There are several innovative methods developed for the detection of CRP with varying degrees of sensitivity.[44,45] The plasmonic ELISA utilizes etched Ag-coated Au nanobipyramids for multicolorimetric detection and achieves an LOD of 0.09 ng/mL.[46] The fluorescent fullerene nanoparticle-based LFIA can detect CRP concentrations between 0.1 and 10 ng/mL in serum in just 15 min.[47] SERS-based lateral flow immunoassay strips, using functionalized Fe_3O_4@Au magnetic nanoparticles, simultaneously detect dual infection biomarkers, with remarkable LODs of 0.1 ng/mL for serum amyloid A and 0.01 ng/mL for CRP.[48] For another SERS-based assay that does not employ magnetoplasmonic particles, a biosensor was constructed comprising DNA three-way junction-conjugated porous Au NPs and an Au−Te nanoworm structure, achieving an LOD of 0.51 ng/mL for CRP in PBS.[49] The ultrasensitive THz metasensor, based on quasi-bound states in the continuum (quasi-BICs), exhibits exceptional sensitivity, detecting biomarkers like CRP and serum amyloid A down to 1 pM (0.12 ng/mL).[50] On the other hand, the electrochemical immunosensor, using indole as an electrochemical probe, demonstrates an LOD of 0.03 ng/mL.[51] The real-time nanoplasmonic immunoturbidimetry assay (NanoPITA) quantifies hypersensitive CRP with a reduced LOD of 0.54 ng/mL.[52] Lastly, a novel smartphone-based device merges magnetoelastic immunosensing and smartphone technology for self-detection of CRP, with an LOD of 0.2349 ng/mL.[53] The summarized comparisons of the biosensors are outlined in Table 2 below.

Table 2. Summary of Methods, Targets, and Their Corresponding LOD Values for CRP Detection

method	target	LOD
conventional ELISA[43,44]	CRP	0.1 ng/mL
plasmonic ELISA[46]	CRP	0.09 ng/mL
fluorescent fullerene nanoparticle-based LFIA[47]	CRP	0.1−10 ng/mL
SERS-based lateral flow immunoassay[48]	CRP	0.01 ng/mL
SERS-based DNA junction-conjugated Au NPs and nanoworms analytical method[49]	CRP	0.51 ng/mL
THz metasensor[50]	CRP	0.12 ng/mL
electrochemical immunosensor[51]	CRP	0.03 ng/mL
nanoplasmonic immunoturbidimetry assay[52]	CRP	0.54 ng/mL
smartphone-based magnetoelastic immunosensing device[53]	CRP	0.2349 ng/mL
magneto-optical Faraday based immunoassay[33]	CRP	0.53 ng/mL
this work	CRP	1.05 fg/mL

CONCLUSIONS

We conducted this experiment by building upon the techniques of functionalizing biochips and synthesizing MPNs previously developed in our laboratory. The main objective was to develop a biomedical detection technology based on SERS measurements with a particular focus on CRP detection. We achieved a highly sensitive LOD for CRP, which was quantified at 5.96 fg/mL.

In response to reproducibility challenges with SERS biochips, we developed a Gaussian binning method integrated with 2D mapping method which can statistically summarize the multiple-location SERS measurement across the sample surface.

Through percentage recovery testing, we confirmed the precision of the experimental results and found that the presence of an external magnetic field had a minimal impact on the percentage of recovery. However, leveraging the exceptional characteristics of MPNs, we explored the possibility of further improving the LOD of our method by employing

https://doi.org/10.1021/acssensors.3c02007
ACS Sens. 2024, 9, 305−314

magnetic fields. As a result, we achieved improved LOD values of 5.74 and 1.05 fg/mL under magnetic fields of 50 and 3700 G, respectively. The current LOD achieved for the CRP assay using our method surpasses the LOD of most detection methods available in the field. Given the extensive range of potential CRP levels in various clinical scenarios, it is important for assays to have high sensitivity, enabling the detection of even the smallest fluctuations in CRP concentration.[31,54] Furthermore, there is increasing focus on the role of CRP in a variety of diseases. The ability to detect ultralow concentrations of CRP could be highly useful in the future.[32,55]

Although in this work, we validated the feasibility and sensitivity of our method by detecting CRP, based on the principles of our chip design, it can be easily modified to detect other types of biomolecules. This research breakthrough not only provides a deeper understanding of SERS biochips but also opens new opportunities for ultrasensitive detection and analysis in various scientific and biomedical applications. By harnessing the potential of MPNs and optimizing the detection parameters, we anticipate even greater advancements in sensitivity and specificity, paving the way for enhanced clinical diagnostics and biomarker detection.

■ ASSOCIATED CONTENT

Supporting Information

The Supporting Information is available free of charge at https://pubs.acs.org/doi/10.1021/acssensors.3c02007.

Information of materials and chemicals used in the article, details of the preparation of the SERS nanotags and SERS immuochip, procedure for incubation, washing, and nanotags application on biochips, spatial representation of the Raman intensity of 1076.5 cm^{-1} peak across 2D Raman mapping, absorption spectra of the nanotags in different stages of synthesis process, TEM images of γ-Fe_2O_3@Au nanoparticles, distribution of the hydrodynamic diameter of γ-Fe_2O_3@Au nanoparticles, SEM images of the SERS immuochip, EDS mapping-based element analysis diagrams of the chip after immunoassay analysis, Raman spectra of the bare biochip without nanotag at various stages, blocking temperature measurements of the MPNs on biochip, and data comparison between single-point SERS measurement and 2D scan SERS mapping with Gaussian binning analysis (PDF)

■ AUTHOR INFORMATION

Corresponding Author

Kuen-Lin Chen − *Department of Physics, National Chung Hsing University, Taichung 402, Taiwan; Institute of Nanoscience, National Chung Hsing University, Taichung 402, Taiwan*; Email: klchen@phys.nchu.edu.tw

Authors

Chin-Wei Lin − *Department of Physics, National Taiwan University, Taipei 106, Taiwan;* orcid.org/0000-0002-1168-6269

Li-Yu Chen − *Department of Physics, National Chung Hsing University, Taichung 402, Taiwan*

Yu-Ching Huang − *Biochemical Technology R&D Center, Ming Chi University of Technology, New Taipei City 243, Taiwan;* orcid.org/0000-0003-4772-8050

Pradeep Kumar − *Department of Physics, National Chung Hsing University, Taichung 402, Taiwan;* orcid.org/0000-0001-6764-5477

Yu-Zhi Guo − *Department of Physics, National Chung Hsing University, Taichung 402, Taiwan*

Chiu-Hsien Wu − *Department of Physics, National Chung Hsing University, Taichung 402, Taiwan; Institute of Nanoscience, National Chung Hsing University, Taichung 402, Taiwan*

Li-Min Wang − *Department of Physics, National Taiwan University, Taipei 106, Taiwan*

Complete contact information is available at: https://pubs.acs.org/10.1021/acssensors.3c02007

Author Contributions

Conceptualization: K.-L.C.; most of the synthesis and measurements: L.-Y.C. and Y.-Z.G.; formal analysis: K.-L.C., L.-Y.C., C.-W.L., and P.K.; investigation: K.-L.C., C.-W.L., L.-Y.C., and Y.-Z.G.; resources: K.-L.C., Y.-C.H., C.-H.W., and L.-M.W.; writing—original draft preparation: K.-L.C., C.-W.L., P.K., and L.-Y.C.; writing—review & editing: K.-L.C., C.-W.L., and Y.-C.H.; and supervision and project administration: K.-L.C.

Notes

The authors declare no competing financial interest.

■ ACKNOWLEDGMENTS

The authors would like to acknowledge the support from the National Science and Technology Council (NSTC) of Taiwan under grants: NSTC 112-2221-E-005-034, NSTC 112-2622-E-131-001, and NSTC 112-2811-M-002-043. We extend our gratitude for the support provided by the MPMS3 SQUID at the Instrumentation Center of National Taiwan University. The TOC graphic and Figure 1 were created with *BioRender.com*.

■ REFERENCES

(1) Le Ru, E. C.; Blackie, E.; Meyer, M.; Etchegoin, P. G. Surface enhanced Raman scattering enhancement factors: a comprehensive study. *J. Phys. Chem. C* **2007**, *111* (37), 13794−13803.

(2) Lai, H.; Xu, F.; Wang, L. A review of the preparation and application of magnetic nanoparticles for surface-enhanced Raman scattering. *J. Mater. Sci.* **2018**, *53* (12), 8677−8698.

(3) Schatz, G. C.; Young, M. A.; Van Duyne, R. P. Electromagnetic mechanism of SERS. In *Surface-enhanced Raman Scattering: Physics and Applications*; Springer, 2006; pp 19−45.

(4) Sharma, B.; Frontiera, R. R.; Henry, A.-I.; Ringe, E.; Van Duyne, R. P. SERS: Materials, applications, and the future. *Mater. Today* **2012**, *15* (1−2), 16−25.

(5) Theiss, J.; Pavaskar, P.; Echternach, P. M.; Muller, R. E.; Cronin, S. B. Plasmonic nanoparticle arrays with nanometer separation for high-performance SERS substrates. *Nano Lett.* **2010**, *10* (8), 2749−2754.

(6) Huang, J.; Zhou, T.; Zhao, W.; Zhang, M.; Zhang, Z.; Lai, W.; Kadasala, N. R.; Liu, H.; Liu, Y. Magnetic-Core−Shell−Satellite Fe_3O_4-Au@ Ag@(Au@ Ag) Nanocomposites for Determination of Trace Bisphenol A Based on Surface-Enhanced Resonance Raman Scattering (SERRS). *Nanomaterials* **2022**, *12* (19), 3322.

(7) Zong, C.; Xu, M.; Xu, L.-J.; Wei, T.; Ma, X.; Zheng, X.-S.; Hu, R.; Ren, B. Surface-enhanced Raman spectroscopy for bioanalysis: reliability and challenges. *Chem. Rev.* **2018**, *118* (10), 4946−4980.

(8) Morton, S. M.; Jensen, L. Understanding the molecule− surface chemical coupling in SERS. *J. Am. Chem. Soc.* **2009**, *131* (11), 4090−4098.

(9) Yang, B.; Jin, S.; Guo, S.; Park, Y.; Chen, L.; Zhao, B.; Jung, Y. M. Recent development of SERS technology: Semiconductor-based study. *ACS Omega* **2019**, *4* (23), 20101−20108.
(10) Hegde, M.; Pai, P.; Shetty, M. G.; Babitha, K. S. Gold nanoparticle based biosensors for rapid pathogen detection: A review. *Environ. Nanotechnol. Monit. Manage.* **2022**, *18*, No. 100756.
(11) Zhang, L.; Mazouzi, Y.; Salmain, M.; Liedberg, B.; Boujday, S. Antibody-gold nanoparticle bioconjugates for biosensors: synthesis, characterization and selected applications. *Biosens. Bioelectron.* **2020**, *165*, No. 112370.
(12) Das, G. M.; Managò, S.; Mangini, M.; De Luca, A. C. Biosensing using SERS active gold nanostructures. *Nanomaterials* **2021**, *11* (10), 2679.
(13) Lee, J.-H.; Cho, H.-Y.; Choi, H. K.; Lee, J.-Y.; Choi, J.-W. Application of gold nanoparticle to plasmonic biosensors. *Int. J. Mol. Sci.* **2018**, *19* (7), 2021.
(14) Liu, H.; Gao, X.; Xu, C.; Liu, D. SERS tags for biomedical detection and bioimaging. *Theranostics* **2022**, *12* (4), 1870.
(15) Yuan, M.; Harnett, M. C.; Yan, T.-H.; Georgas, E.; Qin, Y.-X.; Zhou, H.-C.; Wang, Y. Progress, Opportunities, and Challenges of Magneto-Plasmonic Nanoparticles under Remote Magnetic and Light Stimulation for Brain-Tissue and Cellular Regeneration. *Nanomaterials* **2022**, *12* (13), 2242.
(16) Popov, A. A.; Swiatkowska-Warkocka, Z.; Marszalek, M.; Tselikov, G.; Zelepukin, I. V.; Al-Kattan, A.; Deyev, S. M.; Klimentov, S. M.; Itina, T. E.; Kabashin, A. V. Laser-ablative synthesis of ultrapure magneto-plasmonic core-satellite nanocomposites for biomedical applications. *Nanomaterials* **2022**, *12* (4), 649.
(17) Shibusawa, K.; Hase, T.; Tsukada, K. Increasing surface-enhanced Raman scattering density using gold-coated magnetic nanoparticles controlled via a magnetic field for sensitive and efficient biomarker detection. *AIP Adv.* **2019**, *9* (6), 065316 DOI: 10.1063/1.5102083.
(18) Scaramuzza, S.; Polizzi, S.; Amendola, V. Magnetic tuning of SERS hot spots in polymer-coated magnetic−plasmonic iron−silver nanoparticles. *Nanoscale Adv.* **2019**, *1* (7), 2681−2689.
(19) Huang, H.; Zhang, Z.; Li, G. A Review of Magnetic Nanoparticle-Based Surface-Enhanced Raman Scattering Substrates for Bioanalysis: Morphology, Function and Detection Application. *Biosensors* **2023**, *13* (1), 30.
(20) Liu, Z.; Wang, C.; Zheng, S.; Yang, X.; Han, H.; Dai, Y.; Xiao, R. Simultaneously ultrasensitive and quantitative detection of influenza A virus, SARS-CoV-2, and respiratory syncytial virus via multichannel magnetic SERS-based lateral flow immunoassay. *Nanomed. Nanotechnol. Biol. Med.* **2023**, *47*, No. 102624.
(21) Yin, B.; Ho, W. K. H.; Zhang, Q.; Li, C.; Huang, Y.; Yan, J.; Yang, H.; Hao, J.; Wong, S. H. D.; Yang, M. Magnetic-responsive surface-enhanced Raman scattering platform with tunable hot spot for ultrasensitive virus nucleic acid detection. *ACS Appl. Mater. Interfaces* **2022**, *14* (3), 4714−4724.
(22) Li, D.; Yao, D.; Li, C.; Luo, Y.; Liang, A.; Wen, G.; Jiang, Z. Nanosol SERS quantitative analytical method: A review. *TrAC, Trends Anal. Chem.* **2020**, *127*, No. 115885.
(23) Eskandari, V.; Sahbafar, H.; Zeinalizad, L.; Marashipour, R.; Hadi, A. A review of paper-based substrates as surface-enhanced raman spectroscopy (SERS) biosensors and microfluidic paper-based SERS platforms. *J. Comput. Appl. Mech.* **2022**, *53* (1), 142−156.
(24) Wang, C.; Xu, G.; Wang, W.; Ren, Z.; Zhang, C.; Gong, Y.; Zhao, M.; Qu, Y.; Li, W.; Zhou, H.; Li, Y. Q. Bioinspired hot-spot engineering strategy towards ultrasensitive SERS sandwich biosensor for bacterial detection. *Biosens. Bioelectron.* **2023**, *237*, No. 115497.
(25) Monticone, F.; Alù, A. The quest for optical magnetism: from split-ring resonators to plasmonic nanoparticles and nanoclusters. *J. Mater. Chem. C* **2014**, *2* (43), 9059−9072.
(26) Wang, J.; Li, J.; Zeng, C.; Qu, Q.; Wang, M.; Qi, W.; Su, R.; He, Z. Sandwich-like sensor for the highly specific and reproducible detection of Rhodamine 6G on a surface-enhanced Raman scattering platform. *ACS Appl. Mater. Interfaces* **2020**, *12* (4), 4699−4706.
(27) Li, J.; Wu, J.; Chen, J.; Huang, S.; Liu, J.; Gao, F.; Wang, Y.; Sun, B.; Yu, D.; Sun, J. Dual detection of spinal cord injury biomarkers in rat model using gold nanorod array substrate based on surface-enhanced Raman scattering. *Surf. Interfaces* **2022**, *34*, No. 102400.
(28) Gu, Z.; Tian, S.; Zhou, Q.; Wei, W.; Zhao, L.; Li, X.; Zheng, J. Surface enhanced Raman scattering of molecules related to highly ordered gold cavities. *J. Raman Spectrosc.* **2013**, *44* (12), 1682−1688.
(29) Wang, P.; Wu, L.; Lu, Z.; Li, Q.; Yin, W.; Ding, F.; Han, H. Gecko-inspired nanotentacle surface-enhanced Raman spectroscopy substrate for sampling and reliable detection of pesticide residues in fruits and vegetables. *Anal. Chem.* **2017**, *89* (4), 2424−2431.
(30) Rajab, I. M.; Hart, P. C.; Potempa, L. A. How C-reactive protein structural isoforms with distinctive bioactivities affect disease progression. *Front. Immunol.* **2020**, *11*, 2126.
(31) Luan, Y.-y.; Yao, Y.-m. The clinical significance and potential role of C-reactive protein in chronic inflammatory and neurodegenerative diseases. *Front. Immunol.* **2018**, *9*, 1302.
(32) Ananthula, A.; Konda, M.; Bimali, M.; Safar, A. M.; Govindarajan, R. C-reactive protein (CRP) as a predictive biomarker in lung cancer patients receiving immune checkpoint inhibitors (ICI). *Am. Soc. Clin. Oncol.* **2020**, *38*, e21645 DOI: 10.1200/JCO.2020.38.15_suppl.e21645.
(33) Chen, K.-L.; Lin, Y.-S.; Chen, J.-M.; Wu, C.-H.; Jeng, C.-C.; Wang, L.-M. A sensitive platform for in vitro immunoassay based on biofunctionalized magnetic nanoparticles and magneto-optical Faraday effect. *Sens. Actuators, B* **2018**, *258*, 947−951.
(34) Sun, X.; Li, H. Gold nanoisland arrays by repeated deposition and post-deposition annealing for surface-enhanced Raman spectroscopy. *Nanotechnology* **2013**, *24* (35), No. 355706.
(35) Young, T.; Chang, J.; Ueng, H. Study on annealing effects of Au thin films on Si. *Thin Solid Films* **1998**, *322* (1−2), 319−322.
(36) Natan, M. J. Concluding remarks surface enhanced Raman scattering. *Faraday Discuss.* **2006**, *132*, 321−328.
(37) Ma, N.; Zhang, X.-Y.; Fan, W.; Guo, S.; Zhang, Y.; Liu, Y.; Chen, L.; Jung, Y. M. SERS study of Ag/FeS/4-MBA interface based on the SPR effect. *Spectrochim. Acta, Part A* **2019**, *219*, 147−153.
(38) Li, R.; Lv, H.; Zhang, X.; Liu, P.; Chen, L.; Cheng, J.; Zhao, B. Vibrational spectroscopy and density functional theory study of 4-mercaptobenzoic acid. *Spectrochim. Acta, Part A* **2015**, *148*, 369−374.
(39) McNaught, A. D.; Wilkinson, A. *Compendium of Chemical Terminology*; Blackwell Science: Oxford, 1997.
(40) Saini, R. K.; Sharma, A. K.; Agarwal, A.; Prajesh, R. Near field FEM simulations of plasmonic gold nanoparticle based SERS substrate with experimental validation. *Mater. Chem. Phys.* **2022**, *287*, No. 126288.
(41) Nunes, W. C.; Socolovsky, L.; Denardin, J.; Cebollada, F.; Brandl, A. L.; Knobel, M. Role of magnetic interparticle coupling on the field dependence of the superparamagnetic relaxation time. *Phys. Rev. B* **2005**, *72* (21), No. 212413.
(42) Wang, C. Y.; Yang, T.; Shen, D.; Chen, K.; Chen, J.; Liao, S.; Chieh, J.; Yang, H.-C.; Wang, L. Bioassay using blocking temperature: Interparticle interactions between biofunctionalized magnetic nanoparticles conjugated with biotargets. *Appl. Phys. Lett.* **2017**, *110* (13), 133701 DOI: 10.1063/1.4979142.
(43) Morioka, K.; Sato, H.; Kuboyama, M.; Yanagida, A.; Shoji, A. Quantification of CRP in human serum using a handheld fluorescence detection system for capillary-based ELISA. *Talanta* **2021**, *224*, No. 121725.
(44) Khanmiri, H. H.; Yazdanfar, F.; Mobed, A.; Rezamohammadi, F.; Rahmani, M.; Haghgouei, T. Biosensors; noninvasive method in detection of C-reactive protein (CRP). *Biomed. Microdevices* **2023**, *25* (3), 27.
(45) Balayan, S.; Chauhan, N.; Rosario, W.; Jain, U. Biosensor development for C-reactive protein detection: A review. *Appl. Surface Sci. Adv.* **2022**, *12*, No. 100343.
(46) Weng, G.; Shen, X.; Li, J.; Wang, J.; Zhu, J.; Zhao, J. A plasmonic ELISA for multi-colorimetric sensing of C-reactive protein

by using shell dependent etching of Ag coated Au nanobipyramids. *Anal. Chim. Acta* **2022**, *1221*, No. 340129.
(47) Park, K. M.; Chung, D. J.; Choi, M.; Kang, T.; Jeong, J. Fluorescent fullerene nanoparticle-based lateral flow immunochromatographic assay for rapid quantitative detection of C-reactive protein. *Nano Convergence* **2019**, *6* (1), 35.
(48) Liu, X.; Yang, X.; Li, K.; Liu, H.; Xiao, R.; Wang, W.; Wang, C.; Wang, S. Fe3O4@ Au SERS tags-based lateral flow assay for simultaneous detection of serum amyloid A and C-reactive protein in unprocessed blood sample. *Sens. Actuators, B* **2020**, *320*, No. 128350.
(49) Kim, S. M.; Kim, J.; Yim, G.; Ahn, H. J.; Lee, M.; Kim, T.-H.; Park, C.; Min, J.; Jang, H.; Lee, T. Fabrication of a surface-enhanced Raman spectroscopy-based analytical method consisting of multifunctional DNA three-way junction-conjugated porous gold nanoparticles and Au-Te nanoworm for C-reactive protein detection. *Anal. Bioanal. Chem.* **2021**, *414*, 3197−3204.
(50) Wang, R.; Xu, L.; Huang, L.; Zhang, X.; Ruan, H.; Yang, X.; Lou, J.; Chang, C.; Du, X. Ultrasensitive Terahertz Biodetection Enabled by Quasi-BIC-Based Metasensors. *Small* **2023**, *19*, No. 2301165.
(51) Cheng, Y.-Y.; Feng, X.-Z.; Zhan, T.; An, Q.-Q.; Han, G.-C.; Chen, Z.; Kraatz, H.-B. A facile indole probe for ultrasensitive immunosensor fabrication toward C-reactive protein sensing. *Talanta* **2023**, *262*, No. 124696.
(52) Dang, T.; Li, Z.; Zhao, L.; Zhang, W.; Huang, L.; Meng, F.; Liu, G. L.; Hu, W. Ultrasensitive Detection of C-Reactive Protein by a Novel Nanoplasmonic Immunoturbidimetry Assay. *Biosensors* **2022**, *12* (11), 958.
(53) Yuan, Z.; Han, M.; Li, D.; Hao, R.; Guo, X.; Sang, S.; Zhang, H.; Ma, X.; Jin, H.; Xing, Z.; Zhao, C. A cost-effective smartphone-based device for rapid C-reaction protein (CRP) detection using magnetoelastic immunosensor. *Lab Chip* **2023**, *23* (8), 2048−2056.
(54) Ridker, P. M.; Cook, N. Clinical usefulness of very high and very low levels of C-reactive protein across the full range of Framingham Risk Scores. *Circulation* **2004**, *109* (16), 1955−1959.
(55) Sproston, N. R.; Ashworth, J. J. Role of C-reactive protein at sites of inflammation and infection. *Front. Immunol.* **2018**, *9*, 754.

https://doi.org/10.1021/acssensors.3c02007
ACS Sens. 2024, 9, 305−314